Reinforced silica-carbon nanotube monolithic aerogels synthesised by rapid controlled gelation

Manuel Piñero,[1] María del Mar Mesa-Díaz,[2] Desirée de los Santos,[3] María V. Reyes-Peces,[1] José A. Díaz-Fraile,[4] Nicolás de la Rosa-Fox,[1] Luis Esquivias,[4] Victor Morales-Florez[4*]

[1] Dpto. Física de la Materia Condensada, Universidad de Cádiz, Puerto Real (Spain)
[2] Dpto. Ingeniería Química, Universidad de Cádiz, Puerto Real (Spain)
[3] Dpto. Química-Física, Universidad de Cádiz, Puerto Real (Spain)
[4] Dpto. Física de la Materia Condensada, Universidad de Sevilla, Seville (Spain)

Corresponding author: Dr. Victor Morales-Florez
Dpto. Física de la Materia Condensada, Universidad de Sevilla
Av. Reina Mercedes s/n, E41012 - Seville (Spain)
Email: vmorales@us.es
Phone: +34 9545 55926
ORCID: 0000-0003-4120-2832

Other authors:

Dr. Manuel Piñero, manolo.piniero@uca.es

Dr. María del Mar Mesa-Díaz, mariadelmar.mesa@uca.es

Dr. Desirée de los Santos, desiree.delossantos@uca.es

Mrs. María V. Reyes-Peces, maria.reyes@uca.es

Mr. José A. Díaz-Fraile, josdiafra2@us.es

Dr. Nicolás de la Rosa-Fox, nicolas.rosafox@uca.es

Dr. Luis Esquivias, luisesquivias@us.es

GRAPHICAL ABSTRACT

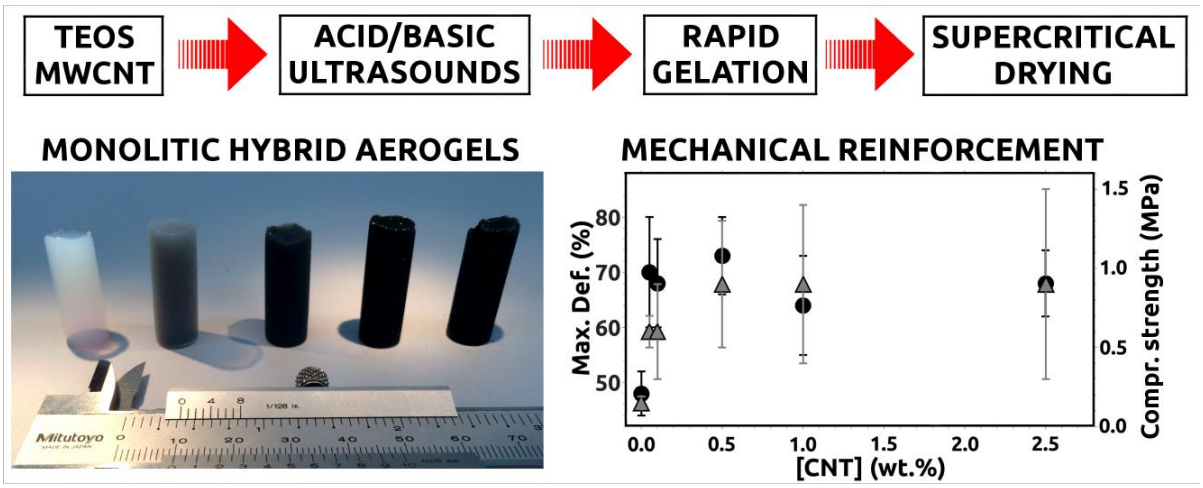

HIGHLIGHTS

• Homogeneous SiO_2–carbon nanotube monolithic aerogels were obtained by rapid controlled gelation

• The carbon nanotubes were homogeneously dispersed in the highly porous silica matrix

• The hybrid aerogels kept outstanding structural features and densities below 80 mg/cm^3 in all cases

• The Si-O-C covalent bonding between carbon nanotubes and silica matrix was prompted by FTIR

• The carbon nanotubes turned the aerogels into 100% stiffer and 60% more deformable materials

ABSTRACT

This work introduces a new synthesis procedure for obtaining homogeneous silica hybrid aerogels with carbon nanotube contents up to 2.50 wt.%. The inclusion of nanotubes in the highly porous silica matrix was performed by a two-step sol-gel process, resulting in samples with densities below 80 mg/cm^3. The structural analyses (N_2 physisorption and SEM) revealed the hierarchical structure of the porous matrix formed by nanoparticles arranged in clusters of 100 nm and 300 nm in size, specific surface areas around 600 m^2/g and porous volumes above 4.0 cm^3/g. In addition, a relevant increase on the mechanical performance was found, and an increment of 50% for the compressive strength and 90% for the maximum deformation were measured by uniaxial compression. This reinforcement was possible thanks to the outstanding dispersion of the CNT within the silica matrix and the formation of Si-O-C bridges between nanotubes and silica matrix, as suggested by FTIR. Therefore, the original synthesis procedure introduced in this work allows the fabrication of highly porous hybrid materials loaded with carbon nanotubes homogeneously distributed in the space, which remain available for a variety of technological applications.

KEYWORDS

Silica hybrid aerogel; carbon nanotube; controlled gelation; structure; reinforcement; mechanical properties.

1. INTRODUCTION

Silica aerogels present outstanding characteristics as host matrix for the performance of the physical or chemical applications of very different embedded phases. The rapid formation of a metal-oxide solid porous network, namely, the formation of the gel or gelation, acts as a glue that immobilizes solid functional phases dispersed into the liquid sol, such as particles, fibres, or nanotubes, that will provide specific applications to the final hybrid material.[1-3] The subsequent supercritical extraction of the liquid preserves the original structure of the solid network of the gel, which results in materials with very low bulk densities (as low as some mg/cm^3), and avoids network changes due to capillary tensions averting solvent exchanges or the use of surfactants which can lead to composite densification due to volume shrinkage.[4,5] These kind of highly porous matrices do not chemically alter their embedded guests and they are stable under very different chemical environments. Besides, silica aerogels exhibit a good thermal stability, typically retain the optical transparency and is featureless throughout most of the UV-vis region.

However, the inherent fragility of the silica aerogels has encouraged large research efforts to increase their mechanical properties and improve their manageability. This has been pursued by chemical additions, but these strategies usually lead to a limitation in the working temperature, an increase in the extreme low density, or a modification of the nanometre-sized hierarchical porosity.[6-8] More recently, aerogel reinforcement has been achieved by embedding solid phases into the silica matrix, such as fibres[9-12] or carbon nanotubes (CNT), which have been frequently considered as a reinforcing phase given that CNT are among the stiffest and strongest fibres known, with Young's moduli as high as 1 TPa and tensile strengths of up to 150 Gpa.[13-15] But, typically, high loads of carbon nanotubes are hindered because they tend to form aggregates owing to string van der Walls force interactions, having this inhomogeneous dispersions a negative effect on the properties of CNT-loaded composites. Nevertheless, the use of basic solutions, the chemical functionalisation, or sonocatalysis[16] (the use of high-power ultrasounds) procedures have improved the dispersion of the CNT in the liquid precursors of the composite facilitating more homogeneous liquid sols and, subsequently, better spatial distributions of the CNT within the porous solid matrix.[14,17-20] In addition, functionalisation could also facilitate the covalent link of the CNT to the silica matrix through the formation of Si-O-C bridges, a relevant issue given that the lack of chemical bonding reduces the effectiveness of the reinforcement.[21-23]

A vast landscape of applications have emerged for CNT thanks to their good versatility of functionalisation, and the sol-gel process has been considered as one of the most common techniques to synthesize CNT-inorganic hybrid composites.[18] Additionally, the structure of the aerogel matrix ensures access for external fluids since it consists of a hierarchical disordered assembly of

nanoparticles in a wide open 3D structure.[10,24-26] Thus, CNT have been encapsulated in functional composites for very different applications, such as optical, thermal, electronic, sensors, biophysics, or environmental.[17,27-32]

Despite the hundreds of articles related to silica-CNT hybrid composites present in the literature, such as glasses,[17] and xerogels,[19,30] or aerogel-like criogels and ambigels,[29,33] just a handful of recent papers focused on aerogels, strictly speaking (obtained by supercritical drying), can be found.[34-37] The aim of this work is to introduce a synthesis procedure to easily obtain monolithic homogeneous silica hybrid aerogels that host functional CNT which may remain available for different applications. In addition, this work deeply researches the structural and mechanical properties of the obtained composites as a function of the CNT content.

2. MATERIALS AND METHODS

2.1 Synthesis procedure

Sols were prepared via acid/basic-catalysed sol-gel two-step process, in an attempt to exert better control over the rates of the hydrolysis and condensation reactions to achieve a rapid controlled gelation procedure that prevents nanotube agglomeration. In Fig. 1, a flow chart summarizes the process. Firstly, 2.5 mL of tetraethoxysilane (TEOS) (Merck, Germany; purity ≥ 99%) were mixed with 2.0 mL of absolute ethanol (Panreac, >99.5%). The mixtures were hydrolysed in acidic water at pH = 1 (HNO_3, Panreac, 60%) under the catalyst effects of ultrasounds, by supplying ultrasonic power for one minute (50 W) Afterwards, 6.5 mL of additional absolute ethanol was added. Next, 3.25 mL of basic solution (pH = 12.00, NH_4OH, Panreac, 30%) were added during 30 s of ultrasound power. This 3.25 mL of basic solution carried the adequate mass of dispersed carbon nanotubes (CNT) corresponding for the targeted CNT wt.% content. This way, the total volume of the sample was kept constant in all samples, regardless the CNT content, in order to build similar silica matrix. Multiwalled CNT (MWCNT) were used (NANOLAB, 15 nm in diameter and 5 μm in length, -COOH functionalised, 95% purity). The basic solutions were prepared with ammonia and 1 h of ultrasound power. All chemical reactions were carried out at room conditions, in a flask immersed in a thermal bath to keep the temperature below 50 ºC during all the process.

Afterwards, the sols gelled in less than five minutes, so the liquid sol is easily poured into cylindrical vials and then closed during this time. The gels were aged at 80 ºC for 48 h, and then the samples were washed daily by soaking in absolute ethanol for 7 days in order to remove traces of unreacted TEOS, nitric acid and ammonia.

Fig. 1 *Flow chart of the synthesis procedure*

Finally, the samples were supercritically dried in an autoclave of 600 mL adding extra ethanol. During this process, temperature was raised at a rate of 1 ºC/min to prevent crossing the vapour-liquid equilibrium line, until T = 260 ºC, which resulted in an increase in pressure to 8 Mpa, ensuring supercritical conditions of ethanol. These conditions were maintained for 30 min, and then the ethanol was isothermally evacuated. Cylinder-shaped hybrid monolithic aerogels with homogeneous embedded CNT were obtained. 75 samples batches were synthesised, for statistics purposes and to check reproducibility, covering a range of CNT content from 0.00 wt.% (pure silica) to 2.50 wt.%.

2.2 Characterization techniques

Density was obtained by measuring the mass and size of the cylindrical samples with a calliper and a microbalance (precision ±0.1 mg). The nanostructural changes occurring in the silica aerogel due to the incorporation of the CNT were investigated by means of N_2 physisorption experiments (Micromeritics ASAP2010, working at 77 K and equipped with pressure transducer resolution of 10^{-4} mm Hg) and by scanning electron microscopy (SEM-FEG, Hitachi S5200), using an acceleration voltage of 5 kV. Prior to N_2 physisorption analyses, samples were milled in an agate mortar and degasified at 150 ºC for 2 h under a N_2 flux. Specific surface area, specific pore volume, pore size and pore size distribution (PSD) were determined considering standard models for the analysis (BET and BJH, respectively). The study on Si-O-C bond formation in the synthesised aerogels were analysed by Fourier transformer infrared spectrophotometry (FTIR). The spectra were recorded in the region from 2000 to 400 cm^{-1} by means of a Bruker Tensor 37 spectrophotometer.

Theoretical structural models have been built according to the works of Esquivias and Rodríguez-Ortega,[24] in order to find a representative geometrical description of the submicrostructure, namely, structural features below 1 μm and above 10 nm. These models are built on the basis of random close packing (RCP) premises, where contact distance and extra porosity can be tuned. They are validated by comparing the experimental PSD with those calculated from models built up using the Monte-Carlo technique, among other strategies. The theoretical PSD are calculated from the largest sphere radius inscribed within the interstices. And the interstice size distribution, *p(K)*, is obtained as function of a reduced variable $K = r/R$, where r is the radius of the largest inscribed sphere and R the particle radius in the hypothesis of hard-sphere approximation. The fitting of the theoretical curves to the experimental data allows characteristic structural parameters such as the characteristic particle size

of a mono-disperse system or the hierarchical levels to be calculated, by simply converting the reduced variable *K* to the real space. Detailed information can be found in the referred article.

Mechanical properties were characterized by uniaxial compression (Shimadzu AG-I Autograph 5 kN) within a ± 1% of indicated test force at 1/250 load cell rating, with a load cell of 500 N using a sample deformation rate of 0.05 mm/min. The mechanical parameters were obtained by unconfined compression from 4 to 5 cylindrical samples ~16.00 mm in height and ~8.00 mm in diameter, fulfilling the ASTM D7012 standard.[38] The flat faces of the cylinders were carefully polished, if necessary. The failure points and the maximum deformation were estimated from the maximum supported load prior to sample failure. The elastic modulus was obtained by the linear slope of the stress-strain loading curve.

3. RESULTS AND DISCUSSIONS

The procedure designed in this work was intended to synthesise homogeneous hybrid gels with a perfect homogenisation of the carbon nanotubes. To achieve this goal, three tools were jointly considered to help a proper dispersion: the use of functionalised CNT within basic solutions, and the use high power ultrasounds, which also helped to enhance the gelation kinetics. Thus, the control of the gelation kinetics with the pH thanks to the addition of the CNT suspensions within the about-to-gel liquid sol involved the formation of homogeneous gels in between 1 and 5 min. Slight decrease of the pH was observed in the basic suspensions, from 12.00 to 11.10, as the CNT concentrations rose. Nevertheless, they were not critical to achieve the rapid controlled gelation and homogeneous gels.

3.1 Physical characterization of the aerogels

Monolithic optically homogeneous samples were obtained up to 2.50 wt.% of CNT content. The designed procedure of rapid gelation has proven to be an effective route to synthesise optically homogeneous CNT-hybrid silica aerogels. In Fig. 2, a sample set is shown.

Fig. 2 *Left: the absence of large agglomeration of CNT and the optical grade of their dispersion throughout the whole sample can be validated in translucent wet hybrid 0.05 wt.% gel; right: samples series just taken out from the supercritical drying ethanol autoclave, with increasing content of CNT, 0.00 wt.%; 0.05 wt.%; 0.50 wt.%; 1.00 wt.% and 2.50 wt.%*

The progressive inclusion of the CNT in the silica porous matrix did not drastically affect the bulk density of the aerogels. Nevertheless, a smooth increase of the density up to 10% upon increasing CNT content, as can be seen in Fig. 3-top, from 68±5 mg/cm^3 for the pure silica samples to 76±15

mg/cm^3 for samples with 2.50 wt.% CNT content. Detailed values can be found in Table 1. This increase can not be explained just in terms of the added CNT mass to the same sample value, given that the maximum loaded sample (2.50 wt.%) would give a density of ~70 mg/cm^3. Therefore, some small densification of the silica matrix was found, most likely due to the presence of increasing CNT contents in the sols that slightly acidified the pH of the CNT basic suspension, from 12.00 down to 11.10 for the highest CNT content. The possible presence of some minor interfacial region of slightly denser silica matrix surrounding the nanotubes[13] was not confirmed by SEM (see next section). In all cases, the density values behaved with increasing CNT content in a similar way to other values reported for silica-CNT aerogels.[35] They remained below the densities of other silica hybrid aerogels,[11] and did not experienced significant increases as reported for ambigels.[27,29]

[CNT] (wt.%)	ρ (mg/cm^3)	S_{BET} (m^2/g)	V_p (cm^3/g)	**Pore size** (nm)
0.00	68 ± 5	520 ± 40	4.3 ± 0.3	20 ± 2
0.10	63 ± 13	480 ± 50	3.9 ± 0.2	23 ± 6
0.50	69 ± 9	540 ± 90	4.1 ± 0.6	20 ± 2
1.00	77 ± 10	650 ± 70	4.0 ± 0.4	17 ± 4
2.00	69 ± 14	570 ± 40	4.4 ± 0.4	20 ± 2
2.50	76 ± 15	630 ± 40	4.6 ± 0.2	19 ± 1

Table 1 *Densities, specific surface area and specific porous volume obtained for the samples series with increasing content of CNT. Pore size stands for the average typical pore size. Error bars represent the standard deviation in all cases. Uncertainties below 20% confirm an acceptable moderate degree of reproducibility*

Thus, the two-step sol-gel procedure permits to exert control on the rates of hydrolysis and condensation reactions, and to design a rapid synthesis procedure for the fabrication of hybrid samples with an outstanding CNT dispersion. Firstly, the acidic hydrolysis takes place in ~1 min in presence of ethanol as homogenizing solvent. And the subsequent addition of the basic CNT-bearing suspension upon high power ultrasound serves a two-fold objective: the stabilisation of the CNT suspension for their homogeneous dispersion within the sol, and the raise of the pH, which increases the gelation kinetics and, along with sonocatalysis, leads to the gelation in a few minutes (between 1 and 5 min) preventing the formation and precipitation of the CNT agglomerates.

3.2 Nanostructure

N_2 physisorption experiments revealed the structural features of the sample series. In Table 1, the values of the specific surface area, specific porous volume and averaged pore size are listed. As a general conclusion, it can be stated that the submicrostucture of the aerogels is not dramatically altered

due to the inclusion of the CNT, regardless the content. Hence, structural parameters such as the specific surface area (Fig. 3-middle and Table 1), specific porous volume or typical pore size (Table 1), do not show neither major changes nor steep trends. Nevertheless, the specific surface area showed a smooth increasing trend upon increasing CNT content, which rose from 520 m^2/g to 630 m^2/g and remained in the typical values for silica aerogels. The negligible contribution of the bare CNT to the S_{BET} was verified by N_2-physisorption experiments to the raw CNT (6 m^2/g for their specific surface area). Therefore, the mentioned small pH variations of the final sol can be responsible of these slight variations.

Fig. 3 *Top: bulk density of the samples for different CNT contents; middle: specific surface area (S_{BET}) vs. CNT content; bottom: pore size distribution of two representative samples with different CNT contents (discontinuous lines), and best fitted theoretical curves (light solid lines) from the hierarchical structural models based on random close packings (sketched in inset)*

Special attention has been paid to the pore size distribution (Fig. 3-bottom). These distributions curves revealed the mesoporous character of the sample, and they also exhibit a well defined peak that indicates a typical pore size of ~16 nm. In addition, this pore size distribution is well explained by the hierarchical structures that describes the silica matrix of the aerogels. This premise was assessed by fitting theoretical PSD curves from structural models (light solid lines in Fig. 3-bottom; see section 'Materials and methods' for details). First of all, no significant changes were observed due to the inclusion of the CNT. Except for small mesopores (<10 nm), for which no good fitting was found, the distribution was successfully described in terms of the composition of theoretical porous distributions from two different hierarchical levels of random packings of sphere-shaped aggregates. Hence, it can be deduced that the structure, below 10 nm, is not well described by arrangements of monosized hard spheres. Instead, basic building particles are far away from the spherical shape and the pores are conformed by particles of different sizes. Finally, the convolution of two of the structural models catalogue[24] was found adequate to satisfactorily fit the distributions between 10 and ~80 nm, indicating that the basic building particles are arranged in a first structural level with clusters of 70.9 mn in size, in an open structure with more than 60% of level porosity with a low coordination number of 3.73. These clusters are subsequently arranged in a third hierarchical level, a denser arrangement with clusters of 211 nm in size and high coordination number (N_{coord} = 8.53). These models were labelled DP20 and HP0, the characteristics of them appear in Table 2.

MODEL	Contact distance	Added Porosity (%)	K_{max}	Particle size (nm)	Φ (%)	N_{Coord}
DP20	0.99	18	0.46	70.9	62	3.73
HP0	0.95	0	0.26	211	40	8.53

Table 2 *Geometrical parameters of the selected structural models which fit the experimental pore size distributions. K_{max}: peak position of the theoretical PSD in reduced units. Particle size is obtained by deconvolution of the peak position. Φ: occupation fraction. N_{coord} stands for coordination number, that is, the average number of first neighbours of the particles in the model*

On the other hand, scanning electron microscopy micrographs revealed submicrostructural features in the morphology of the samples with different CNT contents. In Fig. 4a, the 0.00 wt.% sample presented the well-known disordered hierarchical structure of the porous matrix of the acid-catalysed silica aerogels, in which nanometre non-spherical particles formed clusters subsequently arranged in larger clusters and so on. These features are in coherence with pore size distributions plotted in Fig. 3-bottom and supported the characteristic cluster sizes revealed by the structural models (highlighted in Fig. 4a by dashed circles).

The inclusion of the CNT in the silica matrix can be seen in the micrographs series of Fig. 4b-d. The embedded nanotubes were frequently found linking silica clusters (Fig. 4b), emerging from within the bulk (Fig. 4c), or standing alone (Fig. 4d). At these magnifications, no differences were found between bulk silica matrix and silica of the interfacial region surrounding the nanotubes. In addition, the width of the nanotubes could be checked by analysing high magnification images (inset in Fig. 4d), and sizes below 20 nm were always found, in accordance with the supplier's data. Despite the presence of unwished large agglomerates of CNT cannot be discarded by SEM imaging, they were not found after several SEM imaging sessions. This is in accordance with the excellent optical homogeneity achieved by this original synthesis procedure (Fig. 2).

Fig. 4 *SEM micrographs from samples with different CNT contents: a) texture of the pure silica aerogel matrix, white circles highlight the two typical cluster sizes in the hierarchical arrangement revealed by structural models (see text); b) shows several clusters of nanoporous silica with an embedded single carbon nanotube (pointed by the arrow); c) several nanotubes coated by silica matrix emerged from the bulk; d) a single nanotube is bridging two separated silica clusters; inset: the diameter of the nanotube was verified to be below 20 nm with the help of the ImageJ software. No relevant CNT agglomerates were found. Scale bar stands for 500 nm in all cases, except inset*

3.3 Chemical characterization (FTIR)

FTIR spectra of the samples (Fig. 5) showed the typical SiO_2 vibration bands in range of 400-1100 cm^{-1}, specifically, the band of vibration of Si-O-Si units appears at 472 cm^{-1} (δ(Si-O-Si)), 804 cm^{-1} (ν(Si-O-Si)), 1086 cm^{-1} (ν(Si-O-Si)) and 1107 cm^{-1} (ν_{as}(Si-O-Si)). The band at 966 cm^{-1} could be assigned to Si-OH vibration[39] (ν(Si-OH)). But the relevant differences due to the inclusion of the CNT in the silica matrix are expected in the range of 1000-1100 cm^{-1}. Hence, FTIR spectra exhibited a substantial increase with increasing CNT content at 1096 cm^{-1} (inset in Fig. 5), which suggest the presence of the Si-O-C bonding.[22,23] Despite these FTIR analyses are not conclusive to unambiguously discern the formation of Si-O-C , these evidences strongly suggest the presence of the formation of covalent bonds between the silica matrix and the functionalised carbon nanotubes.

Fig. 5 *Normalized curves of the measured absorbance by FTIR analyses of the pure silica sample (black line) and hybrid silica-CNT samples with the following CNT contents: 0.05 wt.%; 1.00 wt.% and 2.50 wt.% (grey, blue and yellow lines, respectively). Insets magnify the content of the dashed boxes and are focused where evidences of Si-O-C bonds are expected*

3.2 Mechanical properties

The uniaxial compression test revealed the mechanical properties and their dependence with the increasing CNT contents. In Fig. 6, the effect of the inclusion of the CNT in the mechanical properties of the silica aerogel can be observed. Fig. 6a shows four stress-strain representative curves, where it can be observed how the inclusion of the CNT within the silica matrix drastically changes the mechanical behaviour of the samples under uniaxial compression. In contrast to the brittle behaviour of the pure silica aerogel, a stiffening effect in deformations above 50% was found in hybrid samples. The Young's moduli measured at the beginning of the curve revealed a significant stiffening of the samples with 1 wt.% of CNT, and a value of 0.42 Mpa was measured, that is, a ~100% stiffer than pure silica aerogel (0.20 MPa). In addition, these values are one order of magnitude higher than other reported for similar samples[32] remarking the relevance of this new fabrication procedure. Nevertheless, larger contents yielded to a reduction of the Young's modulus (Fig. 6b).

Fig. 6 *Stress-strain curves for selected representative samples (a); dependence of the mechanical parameters determined by uniaxial compression tests with increasing CNT contents (b-d)*

On the other hand, the brittle silica matrix collapsed upon 0.2 Mpa stress and bore less than 50% of deformation (Fig 6c y d) whereas the hybrid samples exhibited an increase of these mechanical parameters reaching compressive strength and maximum deformation values up to 0.9 MPa and 74%, respectively. Hence, they bore up to 6-fold higher loads and 60% larger deformations, an increase close to other reported results for reinforced silica aerogels with silica nanowires.[11] It can be concluded that, regarding the enhancement of the mechanical properties, there is an optimal range of CNT content, between 0.50 and 1.00 wt.%, which leads to the best mechanical performance of the hybrid samples, achieving maximum values of Young's modulus, compressive strength and maximum deformation. Additionally, higher loads of CNT do not imply higher upon uniaxial compression experiments as it occurs in other type of CNT-reinforced materials.

To sum up, the CNT-reinforced silica aerogels have displayed a significant enhancement of the mechanical behaviour in comparison to its pure silica counterpart. The prominent homogeneous dispersion throughout the silica matrix and the bonding between the silica matrix and the carbon nanotubes are making possible the increase of these mechanical values, enabling a route towards the reduction of the extreme fragility of silica aerogels.

4. CONCLUSIONS

Homogeneous silica-CNT hybrid aerogels can be easily obtained by the two-step sol-gel synthesis procedure introduced in this work, thanks to a rapid gelation by controlling pH and the use of high power ultrasounds, which prevent CNT agglomeration. The nanostructure and the density of the samples are not critically affected by the inclusion of nanotubes within the silica porous matrix. Thus, the silica matrix keeps its singular properties after the incorporation of the CNT, such as very low density (below 80 mg/cm^3) and specific surface area (close to 600 m^2/g in all cases) and the open 3D hierarchical nanoparticulate structure. Besides, the good dispersion of the embedded CNT and the intimate structural relationship between CNT and silica characterized by the formation of Si-O-C bridges prompted by FTIR resulted in enhancements greater than 100% of mechanical properties such as the elastic modulus, the maximum deformation or the compressive strength.

In summary, this work introduced a versatile procedure to easily fabricate host porous silica matrices with immobilized CNT as hybrid aerogels, which can be prepared with targeted physical properties beyond structure or mechanical properties, such as thermal, optical or electrical properties, in the view of different applied technological aims.

Acknowledgements

Dr. Miguel Castillo is acknowledged for their wise advises and original ideas. Mr. Alejandro Jurado-Jiménez is acknowledged for his contributions to the starting of this work during his stage at our laboratory. Dr. Alberto Santos and Mr. José Francisco Hidalgo Ramírez are acknowledged for their help in the experimental set-up. The technical staff of the characterization services of the CITIUS (Universidad de Sevilla) is also acknowledged. J.A. D-F. thanks the grant from VI Plan Propio de la Universidad de Sevilla for "starting researchers", M.V. R-P. Thanks the "Programa de contratación de personal técnico de apoyo a la I+D+I 2017" from the Junta de Andalucía (Spain), and V. M-F thanks the postdoctoral grant from the "V Plan Propio de la Universidad de Sevilla". This work has been financed by the support of the Junta de Andalucía (Spain) to the research group TEP-115 (Spain).

Compliance with Ethical Standards

Conflict of interest

The authors declare that they have no competing interests.

References

1. Morris C (1999) Silica Sol as a Nanoglue: Flexible Synthesis of Composite Aerogels. Science 284:622-624. doi: 10.1126/science.284.5414.622

2. Anderson M, Stroud R, Rolison D (2002) Enhancing the Activity of Fuel-cell Reactions by Designing Three-dimensional Nanostructured Architectures: Catalyst-modified Carbon−Silica Composite Aerogels. Nano Letters 2:235-240. doi: 10.1021/nl015707d

3. Warren S, Perkins M, Adams A et al. (2012) A silica sol–gel design strategy for nanostructured metallic materials. Nature Materials 11:460-467. doi: 10.1038/nmat3274

4. Brinker C, Scherer G (1990) Sol-Gel Science, The Physics and Chemistry of Sol-Gel Processing. Academic Press San Diego

5. Aegerter M, Leventis N, Koebel M (2011) Aerogels Handbook Springer New York

6. Leventis N, Sotiriou-Leventis C, Zhang G, Rawashdeh A (2002) Nanoengineering Strong Silica Aerogels. Nano Letters 2:957-960. doi: 10.1021/nl025690e

7. de la Rosa-Fox N, Morales-Flórez V, Toledo-Fernández J et al. (2007) Nanoindentation on hybrid organic/inorganic silica aerogels. Journal of the European Ceramic Society 27:3311-3316. doi: 10.1016/j.jeurceramsoc.2007.02.209

8. Maleki H, Durães L, Portugal A (2014) An overview on silica aerogels synthesis and different mechanical reinforcing strategies. Journal of Non-Crystalline Solids 385:55-74. doi: 10.1016/j.jnoncrysol.2013.10.017

9. Ślosarczyk A, Wojciech S, Piotr Z, Paulina J (2015) Synthesis and characterization of carbon fiber/silica aerogel nanocomposites. Journal of Non-Crystalline Solids 416:1-3. doi: 10.1016/j.jnoncrysol.2015.02.013

10. Zhao S, Zhang Z, Sèbe G et al. (2015) Multiscale Assembly of Superinsulating Silica Aerogels Within Silylated Nanocellulosic Scaffolds: Improved Mechanical Properties Promoted by Nanoscale Chemical Compatibilization. Advanced Functional Materials 25:2326-2334. doi: 10.1002/adfm.201404368

11. Tang X, Sun A, Chu C et al. (2017) A novel silica nanowire-silica composite aerogels dried at ambient pressure. Materials & Design 115:415-421. doi: 10.1016/j.matdes.2016.11.080

12. Hou X, Zhang R, Fang D (2018) An ultralight silica-modified ZrO 2 –SiO 2 aerogel composite with ultra-low thermal conductivity and enhanced mechanical strength. Scripta Materialia 143:113-116. doi: 10.1016/j.scriptamat.2017.09.028

13. Coleman J, Khan U, Blau W, Gun'ko Y (2006) Small but strong: A review of the mechanical properties of carbon nanotube–polymer composites. Carbon 44:1624-1652. doi: 10.1016/j.carbon.2006.02.038

14. Esawi A, Farag M (2007) Carbon nanotube reinforced composites: Potential and current challenges. Materials & Design 28:2394-2401. doi: 10.1016/j.matdes.2006.09.022

15. Liu Y, Ramirez C, Zhang L et al. (2017) In situ direct observation of toughening in isotropic nanocomposites of alumina ceramic and multiwall carbon nanotubes. Acta Materialia 127:203-210. doi: 10.1016/j.actamat.2017.01.024

16. Esquivias L, Piñero M, Morales-Flórez V, de la Rosa-Fox N (2011) In: Aegerter M, Leventis N, Koebel M (eds) Aerogels Handbook. Springer New York. doi:10.1007/978-1-4419-7589-8

17. Berguiga L, Bellessa J, Vocanson F et al. (2006) Carbon nanotube silica glass composites in thin films by the sol–gel technique. Optical Materials 28:167-171. doi: 10.1016/j.optmat.2005.03.002

18. Eder D (2010) Carbon Nanotube−Inorganic Hybrids. Chemical Reviews 110:1348-1385. doi: 10.1021/cr800433k

19. López A, Ureña A, Rams J (2011) Wear resistant coatings: Silica sol–gel reinforced with carbon nanotubes. Thin Solid Films 519:7904-7910. doi: 10.1016/j.tsf.2011.05.076

20. Yusof Y, Johan M (2014) Concentration-dependent properties of amorphous carbon nanotube/silica composites via the sol–gel technique. CrystEngComm 16:8570-8575. doi: 10.1039/c4ce01083c

21. Loo S, Idapalapati S, Wang S et al. (2007) Effect of surfactants on MWCNT-reinforced sol–gel silica dielectric composites. Scripta Materialia 57:1157-1160. doi: 10.1016/j.scriptamat.2007.07.040

22. OH t, Choi C (2010) Comparison between SiOC Thin Film by plasma enhance chemical vapor deposition and SiO2 Thin Film by Fourier Transform Infrared Spectroscopy. Journal of the Korean Physical Society 56:1150-1155. doi: 10.3938/jkps.56.1150

23. Hassan M, Takahashi T, Koyama K (2013) Preparation and characterisation of SiOC ceramics made from a preceramic polymer and rice bran. Journal of the European Ceramic Society 33:1207-1217. doi: 10.1016/j.jeurceramsoc.2012.11.027

24. Esquivias L, Rodriguez-Ortega J, Barrera-Solano C, De La Rosa-Fox N (1998) Structural models of dense aerogels. Journal of Non-Crystalline Solids 225:239-243. doi: 10.1016/s0022-3093(98)00123-9

25. Morales-Flórez V, Piñero M, de la Rosa-Fox N et al. (2008) The cluster model: A hierarchically-ordered assemblage of random-packing spheres for modelling microstructure of porous materials. Journal of Non-Crystalline Solids 354:193-198. doi: 10.1016/j.jnoncrysol.2007.07.061

26. Amonette J, Matyáš J (2017) Functionalized silica aerogels for gas-phase purification, sensing, and catalysis: A review. Microporous and Mesoporous Materials 250:100-119. doi: 10.1016/j.micromeso.2017.04.055

27. Zamora-Ledezma C, Añez L, Primera J et al. (2008) Photoluminescent single wall carbon nanotube–silica composite gels. Carbon 46:1253-1255. doi: 10.1016/j.carbon.2008.04.020

28. Vila M, Hueso J, Manzano M et al. (2009) Carbon nanotubes—mesoporous silica composites as controllable biomaterials. Journal of Materials Chemistry 19:7745. doi: 10.1039/b909628k

29. Bargozin H, Amrikhani L, Moghaddas JS, Ahadian MM (2010) Synthesis and applications of silica aerogel-MWCNT nanocomposites for adsorption of organic pollutants. Transaction F: Nanotechnology 17:122-132.

30. Duque J, Gupta G, Cognet L et al. (2011) New Route to Fluorescent Single-Walled Carbon Nanotube/Silica Nanocomposites: Balancing Fluorescence Intensity and Environmental Sensitivity. The Journal of Physical Chemistry C 115:15147-15153. doi: 10.1021/jp2012107

31. Shearer C, Cherevan A, Eder D (2014) Application and Future Challenges of Functional Nanocarbon Hybrids. Advanced Materials 26:2295-2318. doi: 10.1002/adma.201305254

32. Sivakumar R, Guo S, Nishimura T, Kagawa Y (2007) Thermal conductivity in multi-wall carbon nanotube/silica-based nanocomposites. Scripta Materialia 56:265-268. doi: 10.1016/j.scriptamat.2006.10.025

33. Ślosarczyk A (2017) Synthesis and characterization of silica aerogel-based nanocomposites with carbon fibers and carbon nanotubes in hybrid system. Journal of Sol-Gel Science and Technology 84:16-22. doi: 10.1007/s10971-017-4470-4

34. Hamilton C, Chavez M, Duque J et al. (2010) Carbon Nanomaterials in Silica Aerogel Matrices. MRS Proceedings 1258. doi: 10.1557/proc-1258-r05-11

35. Duque J, Hamilton C, Gupta G et al. (2011) Fluorescent Single-Walled Carbon Nanotube Aerogels in Surfactant-free Environments. ACS Nano 5:6686-6694. doi: 10.1021/nn202225k

36. Chernov A, Predein A, Danilyuk A et al. (2016) Optical properties of silica aerogels with embedded multiwalled carbon nanotubes. physica status solidi (b) 253:2440-2445. doi: 10.1002/pssb.201600326

37. Menshutina N, Ivanov S, Tsygankov P, Khudeev I (2017) Synthesis and characterization of composite materials “aerogel-MWCNT”. Journal of Sol-Gel Science and Technology 84:382-390. doi: 10.1007/s10971-017-4474-0

38. ASTM D7012-14e1 (2014) Standard Test Methods for Compressive Strength and Elastic Moduli of Intact Rock Core Specimens under Varying States of Stress and Temperatures, ASTM International West Conshohocken PA USA. doi:10.1520/D7012-14E01

39. Dervin S, Lang Y, Perova T et al. (2017) Graphene oxide reinforced high surface area silica aerogels. Journal of Non-Crystalline Solids 465:31-38. doi: 10.1016/j.jnoncrysol.2017.03.030

Figure 1

Click here to download Figure FIG1_Diagram.eps

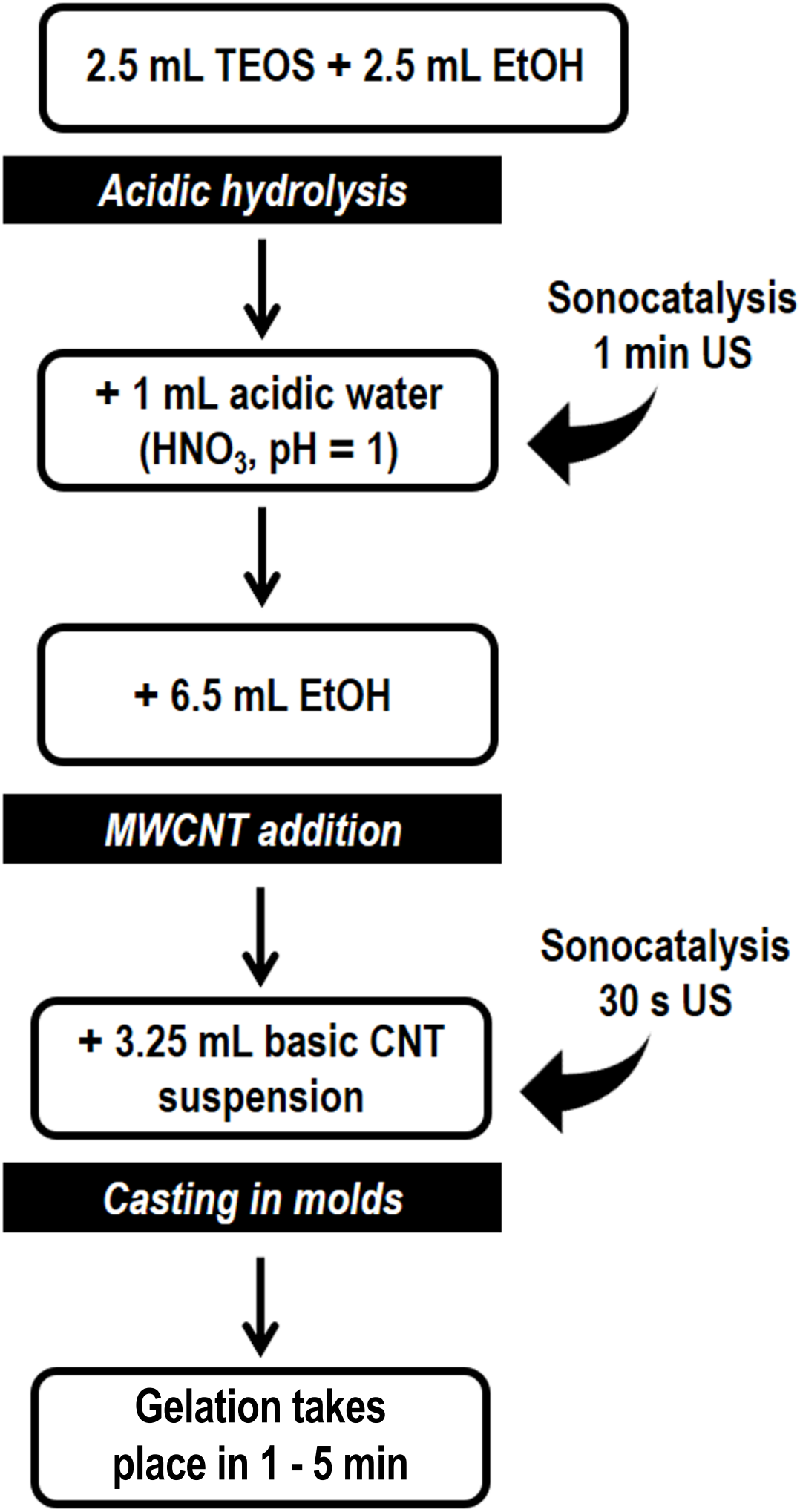

Figure 2

Click here to download Figure FIG2_Samples_JSST.tif

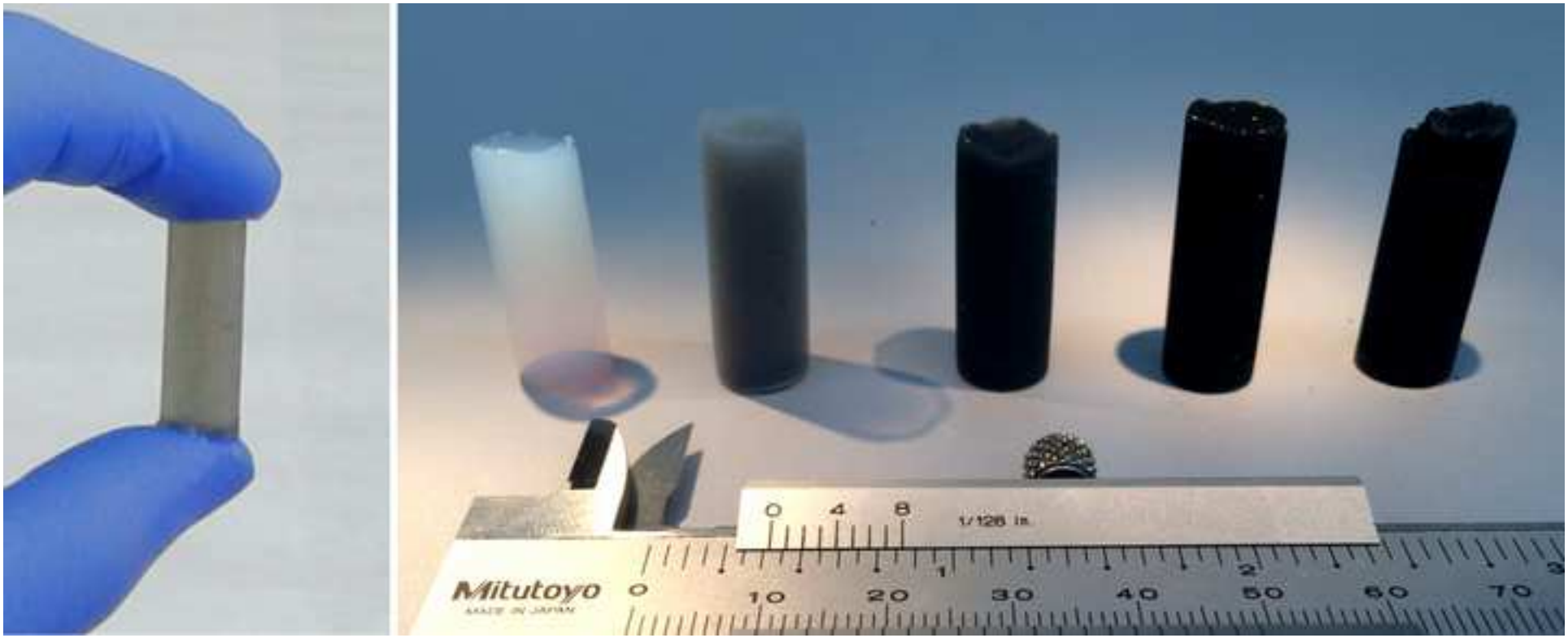

Figure 3

Click here to download Figure FIG3_N2.eps

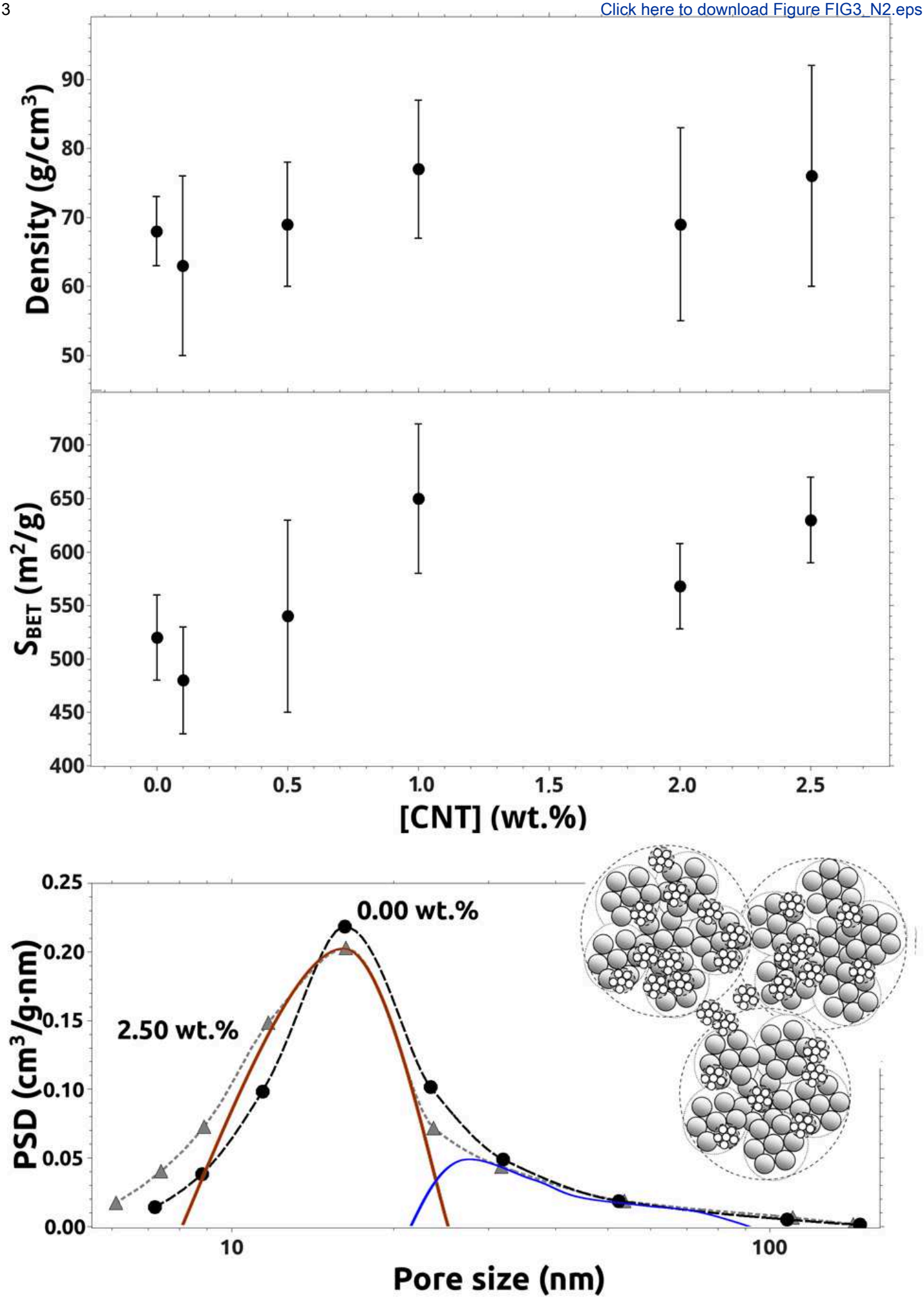

Figure 4

Click here to download Figure FIG4_SEM_JSST.eps

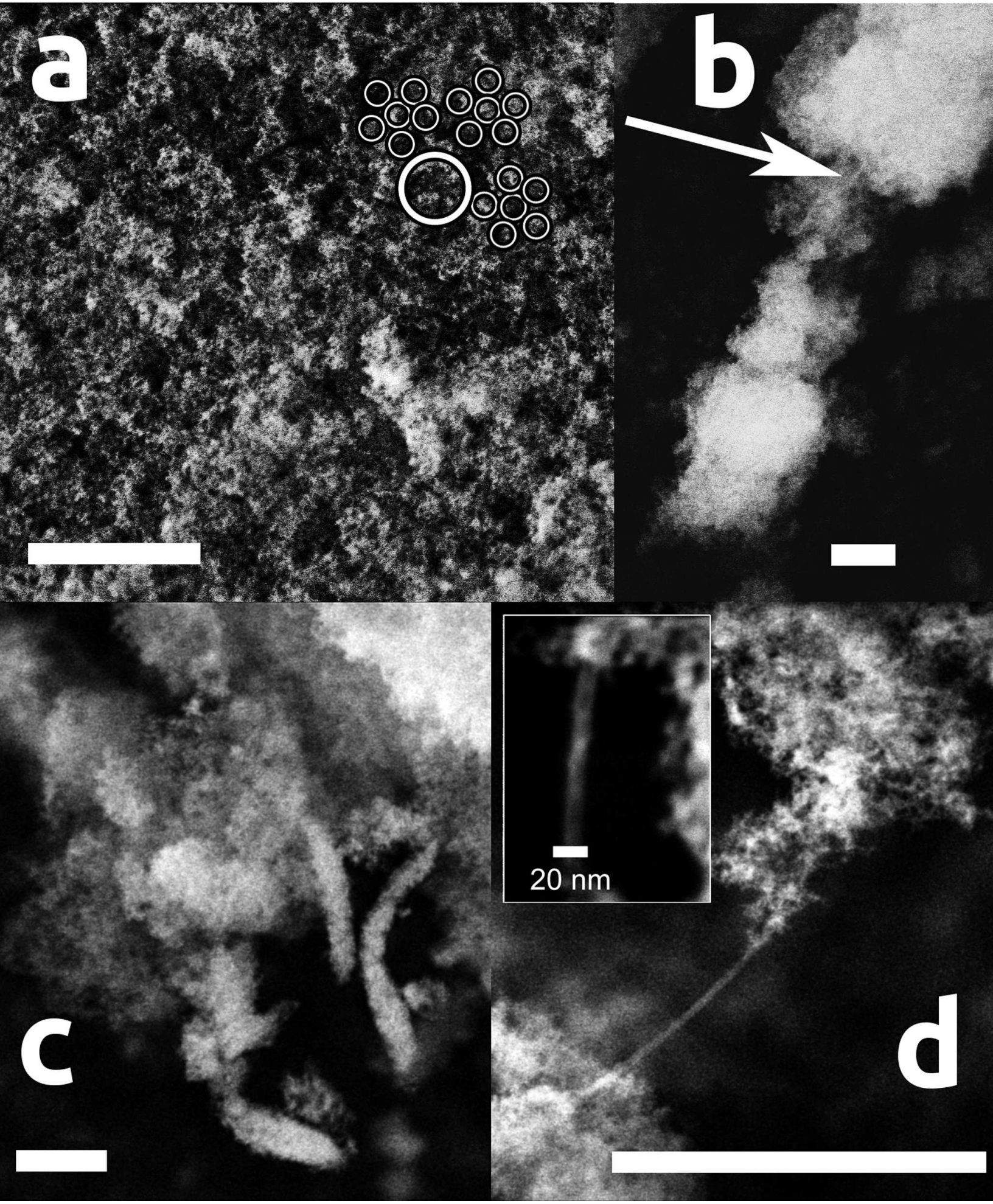

Figure 5

Click here to download Figure FIG5_FTIR.eps

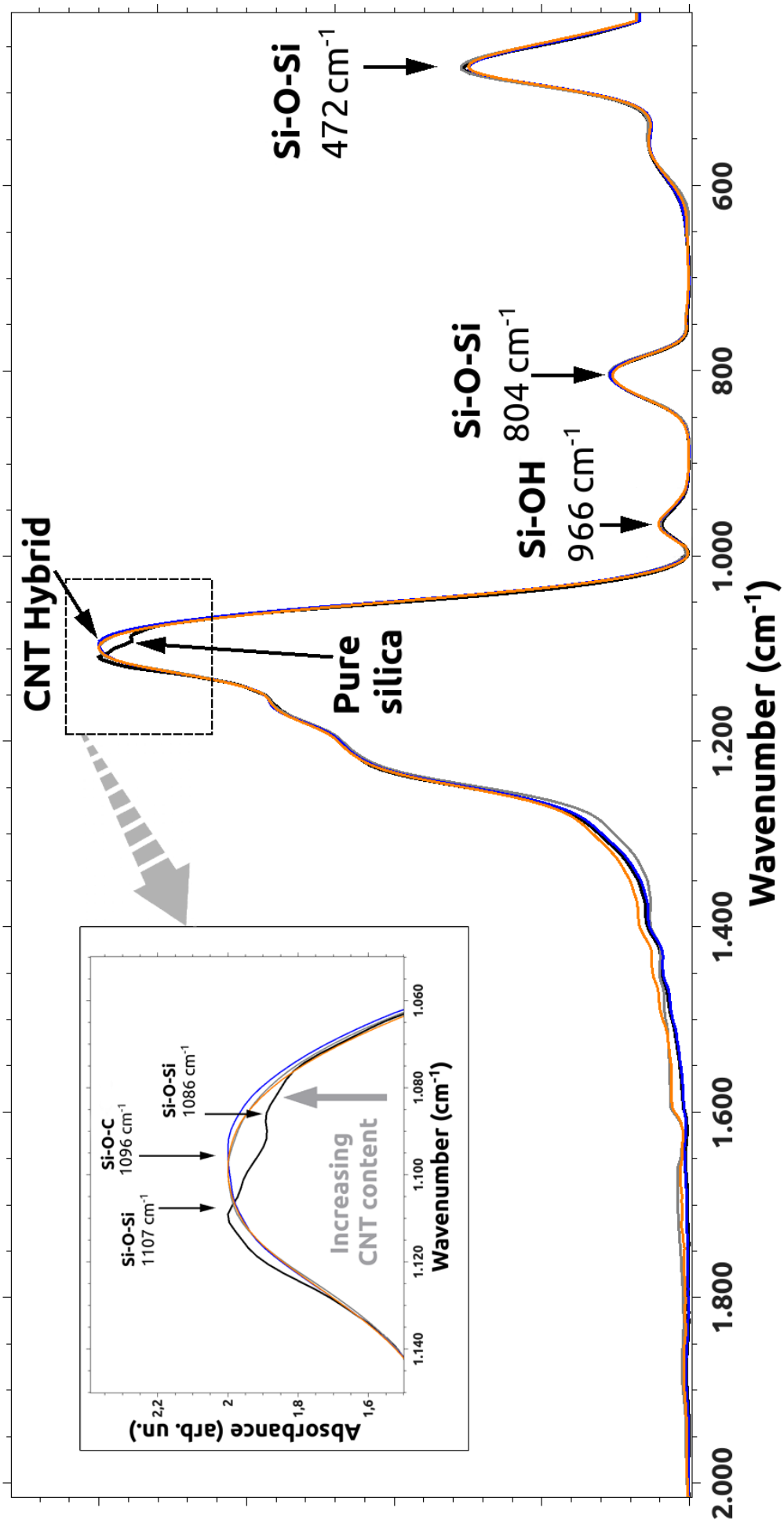

Figure 6

Click here to download Figure FIG6_Mecanicas.eps